

The Effects of Surface Contamination on Resistance Degradation of Hot-Switched Low-Force MEMS Electrical Contacts

Daniel J. Dickrell III
Sandia National Laboratories*
Albuquerque, NM, USA

Michael T. Dugger
Sandia National Laboratories
Albuquerque, NM, USA

Abstract— This work investigated the relationship between the resistance degradation in low-force metal contacts and hot-switched operational conditions representative of MEMS devices. A modified nano-indentation apparatus was used to bring electrically-biased gold and platinum surfaces into contact at a load of 100 μN . The applied normal force and electrical contact resistance of the contact materials was measured simultaneously. The influence of parallel discharge paths for stored electrical energy in the contact circuit is discussed in relation to surface contamination decomposition and the observed resistance degradation.

Keywords—MEMS; contamination; hot-switched; degradation; gold; platinum; arcing;

I. INTRODUCTION

The performance and reliability of microelectromechanical systems (MEMS) that utilize dynamically operating electrical contacts depends critically on the ability of the contact interface to remain as conductive and non-adherent as possible. Surface contamination is a known cause of MEMS electrical contact failure due to highly resistive surface species that retard current flow [1]. MEMS electrical contacts are also particularly susceptible to surface contamination effects as the contact forces available to disrupt thin surface films are significantly constrained by actuator force limitations.

The sources of contamination affecting MEMS electrical contacts are varied. Some can be native to the surface, such as an oxide, or of foreign origin, such as adsorbed species [2]. One process of *in-situ* contaminant formation involves the energetic decomposition of existing contaminant species into highly resistive compounds [3]. The cyclic degradation of certain electrical contacts has been attributed to this cause [4]. Hot-switched contact arcing has been proposed as a sufficiently energetic cause to decompose surface contaminants and impact surface conductivity [5-6]. An understanding of these degradation processes affecting MEMS electrical contacts and development of methods to control them would be beneficial to developers and users of microscale electrical devices. This work investigates how the degradation of hot-switched, low force metal contacts is affected by surface contaminant decomposition and also how the degradation can be circumvented.

*Sandia is a multi-program laboratory operated by Sandia Corporation, a Lockheed Martin Company, for the United States Department of Energy's National Nuclear Safety Administration under contract DE-AC04-94AL85000.)

Apparatus Schematic

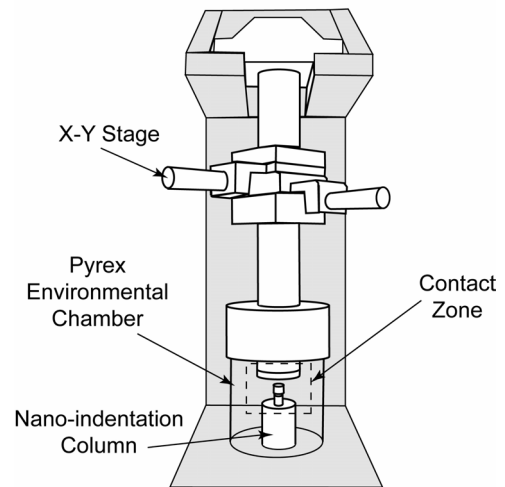


Figure 1. Diagram of the modified nanoindenter apparatus

II. EXPERIMENT

Contact resistance testing of a metal coated sphere-on-flat geometry was performed using a modified nano-indentation test platform. Schematic diagrams of the experimental apparatus and contact zone are shown in Figs. 1 and 2. The apparatus measured the force applied to, and displacement of, the sphere electrode. The apparatus also simultaneously recorded contact resistance determined from the voltage drop measured across the contact and a known sourced current. The voltage drop was assessed via a 4-wire measurement technique. The open-circuit voltage limit across the contact was set to 3.3 V and current source was set to 3 mA. These conditions were specifically chosen to mimic a hot-switched MEMS-based environmental sensing device.

The contact materials studied were a gold-platinum contact pair. The sphere samples were 1.6 mm diameter and made of Si_3N_4 . The spheres were sputter-coated with a 100 nm thick titanium adhesion layer followed by a 500 nm gold contact layer. Silicon wafer flats were sputter-coated with a mixed titanium-titanium nitride adhesion/barrier layer that was 120 nm thick. The purpose of the reactively sputtered titanium nitride layer was to prevent unwanted modification of the contact surface properties by interlayer diffusion. A 200 nm

thick Pt contact layer was deposited last as the primary electrode material on the flat sample. Contact surfaces were cleaned with an ultrasonic acetone wash, followed by an ultrasonic methanol wash and post-wash UV-ozone clean to remove any latent contamination from the wash.

Contact Zone Schematic

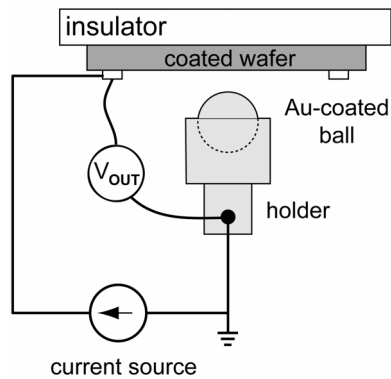


Figure 2. Contact zone diagram showing electrode geometry and contact resistance measurement

The as-deposited root-mean-square roughness of the coated spheres and wafers were measured by white-light interferometry to be 11.3 nm and 2.8 nm, respectively. A stainless steel and Pyrex environmental enclosure was constructed to test in inert gaseous environments. This enclosure isolated the area immediately around the contact and attained an oxygen concentration of 3 ppm when filled with flowing nitrogen. The experimental apparatus resided in a class 1,000 clean room at 22 ± 3 degrees Celsius and $30 \pm 10\%$ relative humidity.

A single contact cycle consisted of several steps. The two electrodes were brought into contact at a controlled load rate of $20 \mu\text{N/s}$ until the maximum target load of $100 \mu\text{N}$ was reached. The load was then held for 3 seconds while an average peak-load resistance value was calculated. The contact was then unloaded at the same rate until the contacts separated. The load required to physically separate the contact surfaces was stored as the pull-off force. Fig. 3 shows an example of one contact cycle. This process was repeated in order to detect cyclical changes in contact resistance and pull-off force for the hot-switched low-force Au-Pt contact.

III. RESULTS

Fig. 4 shows the cyclic resistance degradation of the Au-Pt contact pair under hot-switched conditions. The initial measured contact resistance was 2.2Ω , a higher resistance than what is predicted using the simple equation $R = \rho / 2a$, where ρ is the mean resistivity and a is the contact radius obtained from assuming plastic contact. The large initial resistance is most likely from surface films contributing to the measured value, a fact which is neglected in the equation shown above.

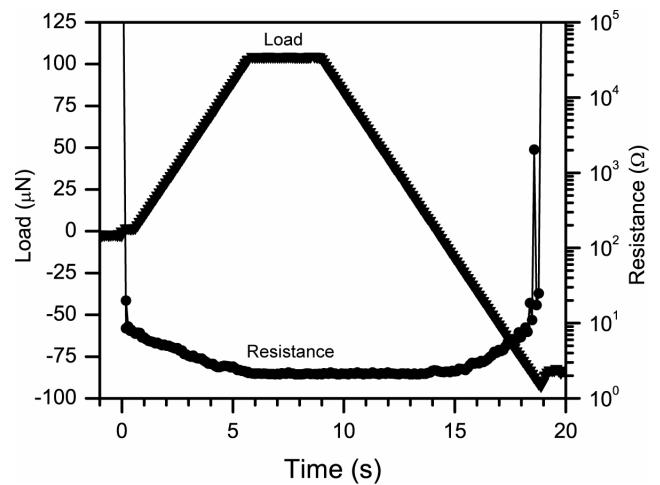


Figure 3. Example of one hot-switched contact cycle

Hot-switched contact arcing has been proposed as a mechanism that can decompose adsorbed surface contaminants. While there was no visually apparent evidence of arcing occurrence upon post-experiment examination, this hypothesis was investigated by placing an RC circuit element in parallel to the contact. The rationale for using the capacitive-quench has been described previously as an alternative discharge path for any stored energy upon contact make and break [7]. The specific values used for the resistive and capacitive elements were 1000Ω and $0.1 \mu\text{F}$, respectively. The effect of placing the capacitive-quench in parallel to the contact is shown in Fig. 5. A more illustrative experiment was conducted where the capacitive-quench was active from the beginning of hot-switched testing, but later removed to observe the effects on the resistance degradation. The results of this experiment are shown in Fig. 6. The grey area in Fig. 6 denotes the cycles where the quench was removed beginning at cycle 75.

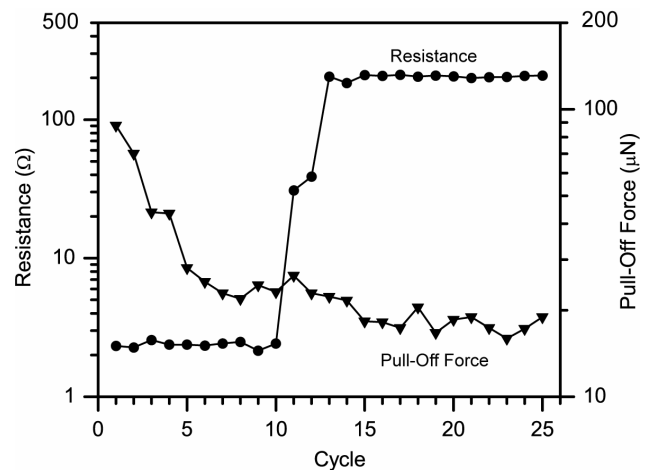


Figure 4. Cyclic contact resistance degradation and diminishing pull-off force

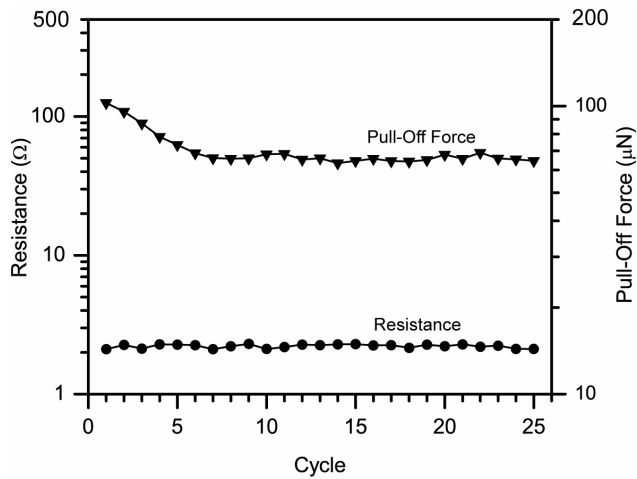


Figure 5. Effect of placing arc-quenching RC element in parallel with contact

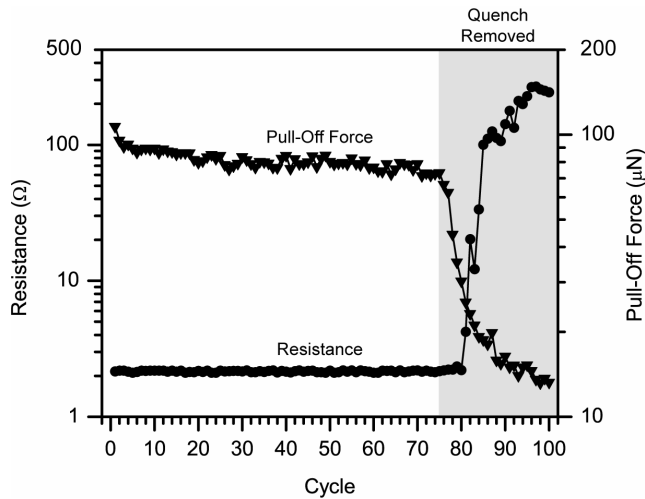


Figure 6. Effect of removing capacitive-quench on contact resistance degradation at cycle 75

Post-experimental contact surface analysis was performed using Time-Of-Flight Secondary-Ion Mass Spectroscopy (TOF-SIMS) and Auger Electron Spectroscopy (AES). Unfortunately, there was no apparent evidence on the contact surfaces, such as surface damage or discoloration, that indicated where to perform elemental species analysis. This made the direct correlation of the measured resistance degradation to changes in surface composition caused by arcing or surface heating unattainable.

IV. DISCUSSION

The effect of the capacitive-quench on the measured contact resistance degradation is quite apparent. While the quench is in parallel with the contact the resistance and pull-off force remain relatively constant. When the quench is removed the contact resistance begins to degrade significantly in a period of only several contact cycles. The attendant decrease in measured pull-off force supports the hypothesis that something is formed in the contact interface that is more resistive and less adherent than the bare metal contact. Another interesting aspect

of Fig. 6 is that for a few, brief cycles before the rapid increase in contact resistance the pull-off force is already decreasing sharply. This effect can also be seen in Fig. 4.

A simple model to describe the measured contact behavior is proposed. The contact areas that support loads typical of MEMS contacts have been posed as small in size, on the order of hundreds of nanometers in diameter, and finite in number, ranging from $N = 10 \sim 100$ individual areas [8]. These small islands of metal contact are responsible for both the interfacial adhesion and electrical current transmission. The contact resistance of a rough surface contact can be expressed similarly to a network of parallel resistors, shown in (1). The expression for an individual resistor in the network is shown in (2).

$$\frac{1}{R_c} = \sum_{i=1}^N \frac{1}{R_i} \quad (1)$$

$$R_i = \frac{\rho}{2a} + \frac{(\rho_f)t}{\pi a^2} \quad (2)$$

The first term in (2) is classical constriction resistance of a circular metallic junction of resistivity ρ and radius a . The second term adds the resistance contribution from a film of resistivity ρ_f and thickness t .

The adhesive force of the same rough surface contact may be treated of as a collection of interfacial bonding forces that sum to give an overall pull-off force, shown in (3). One method of expressing the adhesive force of a single asperity contact is shown in (4) [9]. Equation (4) contains the interfacial surface energy and asperity radius, γ and r , respectively.

$$F_{po} = \sum_{i=1}^N |F_i| \quad (3)$$

$$F_i = -\frac{3}{2} \gamma \pi r \quad (4)$$

Using these expressions, an estimate of how arc-induced contaminant decomposition would affect the pull-off force and contact resistance was performed. Assuming there are a finite number of metal contact areas, N , with the same radius and resistivity, arc-induced decomposition of surface contamination will result in an increase of the film resistivity in (2) and a decrease of the surface energy terms in (4). After each cycle an additional contact area is “contaminated” by an arc-event and the resistivity and surface energy are modified for that contact. Fig. 7 and 8 show how the simulated effects of surface arcing correspond with the measured data for contact resistance and pull-off force from Fig. 4 for different values of N . The film thickness is assumed to remain constant for simplicity.

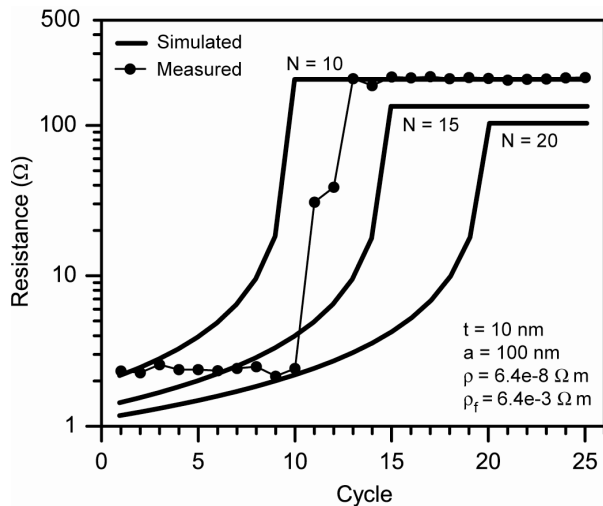


Figure 7. Simulated contact resistance degradation using (1) and (2) vs. measured contact resistance degradation from Fig. 4

It should be stated that the models proposed are not meant for absolute quantitative comparison to the experimentally measured data, but intended more to further clarify the hypothesized processes responsible for the observed contact behavior. A significant amount of freedom exists in choosing what inputs to use in the degradation simulation, suggesting that a wide range of outcomes are possible. However, the model input values were chosen to embody the physical reality of the experiment as well as could be determined.

For example, surface contaminant film thickness, t , was determined from AES. The analysis showed a significant carbon peak at the surface. However, the existing carbon film was not thick enough to obscure the Auger peak of the underlying Pt metal. This indicated that the maximum adsorbed film thickness was on the order of 10 nm, as a thicker film would render the Pt peak undetectable while a thinner film would not be as strongly detected. The resistivity value used for the uncontaminated contact was the average bulk resistivity for Au and Pt. The contaminated contact resistivity was harder to assess, but values for ρ_f have been previously estimated for carbonaceous surface contaminants [3]. Using these estimates, an explanation for the observed contact resistance degradation behavior was proposed using the simple arc-induced contamination models outlined in (1-4).

V. CONCLUSION

The contact resistance degradation of a hot-switched low-force Au-Pt contact typical of MEMS electrical contacts was investigated using a modified nano-indentation apparatus. The contact resistance increased by two orders of magnitude over the initial resistance in only 5 to 10 cycles. The measured pull-off force also decreased by an order of magnitude, suggesting that the electrical contact surface was being contaminated *in-situ*. The contamination-forming process, and thereby the resistance degradation, was circumvented by placing an arc-

quenching RC element in parallel to the contact that provided an alternative discharge path for stored electrical energy at contact make and break. The hypothesis of sequential contact area contamination was simulated, using a simple model of the degradation process. Although containing several adjustable parameters, this simple model predicted trends that agree well with observed behavior when reasonably valued model parameters were chosen.

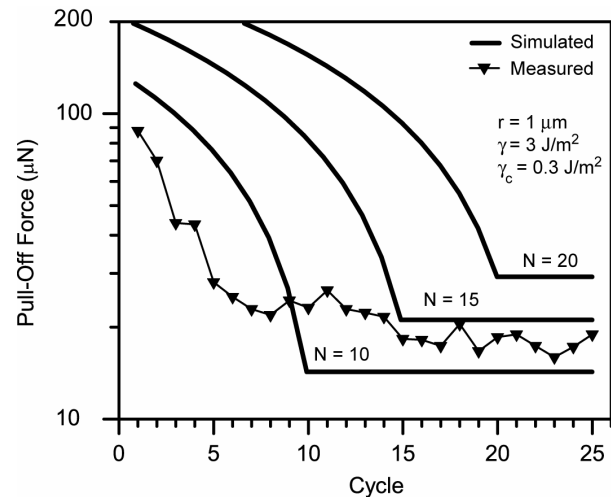


Figure 8. Simulated pull-off force using (3) and (4) vs. measured pull-off force from Fig. 4

REFERENCES

- [1] Schimkat, J., 1999, "Contact Measurements Providing Basic Design Data for Microrelay Actuators," *Sensors and Actuators – A*, 73, pp. 138-143.
- [2] Tringe, J.W., Uhlman, T.A., Oliver, A.C., and Houston, J.E., 2003, "A Single Asperity Study of Au/Au Electrical Contacts," *Journal of Applied Physics*, 93(8), pp. 4661-4669.
- [3] Wang, B., Saka, N., and Rabinowicz, E., 1992, "The Failure Mechanism of Low-Voltage Electrical Relays," *Electrical Contacts - 1992. Proceedings of the Thirty-Eighth IEEE Holm Conference on Electrical Contacts*, pp. 191-202.
- [4] Neufeld, C.N., and Rieder, W.F., 1995, "Electrical Characteristics of Various Contact Contaminations," *IEEE Transactions on Components, Packaging, and Manufacturing Technology – Part A*, 18(2), pp. 369-374.
- [5] Gray, E.W., 1976, "The Particles of Contact Activation," *IEEE Transactions on Parts, Materials, and Packaging*, 12(1), pp. 11-15.
- [6] Tamai, T., 1995, "Effect of Silicone Vapour and Humidity on Contact Reliability of Micro Relay Contacts," *IEEE Transactions on Components, Packaging, and Manufacturing Technology – Part A*, 19(3), pp. 329-338.
- [7] Holm, R., 1967, *Electric Contacts: Theory and Application*, Springer-Verlag, New York.
- [8] Majumder, S., McGruer, N.E., Adams, G.G., Zavracky, P.M., Morrison, R.H., and Krim, J., 2001, "Study of Contacts in an Electrostatically Actuated Microswitch," *Sensors and Actuators – A*, 93, p. 19-26.
- [9] Johnson, K.L., Kendall, K., and Roberts, A.D., 1971, "Surface Energy and the Contact of Elastic Solids," *Proceedings of the Royal Society of London. Series A. Mathematical and Physical Sciences*. 324(1558), pp. 301-3.